The Interaction of Symmetric and Asymmetric Modes in a High-Power Traveling-Wave Amplifier

Samer Banna, *Member, IEEE*, John A. Nation, *Fellow, IEEE*, Levi Schächter, *Senior Member, IEEE*, and Pingshan Wang, *Member, IEEE*

***Abstract*—A three-dimensional (3-D) model has been developed for the investigation of the coupling of the lowest symmetric and asymmetric modes in a high-power, high-efficiency traveling-wave amplifier. We show that in a uniform structure and for an initially nonbunched beam, the interaction efficiency of the asymmetric mode may be much higher than that of the symmetric mode. It is also shown that the coupling between these two modes is determined by a single parameter that depends on the beam characteristics; its value varies between zero when no coupling exists and unity in case of maximum coupling. For a beam that is uniform at the input end, this parameter varies linearly with the guiding magnetic field. In case of a bunched beam, it decreases linearly with the increasing phase-spread of the bunch. Because of the interaction, the radius of the beam increases linearly with the power associated with the asymmetric mode at the input end; it increases rapidly in the case of an initially uniform beam relative to the case of a prebunched beam. Selective damping to suppress the asymmetric mode is described and analyzed.**

***Index Terms*—Amplification of radiation, asymmetric mode, electron acceleration, hybrid mode.**

I. Introduction

In THE recent years, a significant amount of experimental and theoretical effort has been directed toward generation of high-power, high-efficiency microwave in various laboratories, universities, and industries around the world (SLAC [1]–[3], CERN [4], KEK [5], LLNL [6], NRL [7]–[9], IAP [10], [11], US-Air Force Labs. [12], University of Maryland [13], Cornell University [14]–[22], CPI, Litton, Thomson [23], HRC [24]–[26], Omega-P [27], FMT [28], and others). Many efforts have been directed toward improving the systems' efficiency and at the same time increasing their operation frequency. These two goals set a significant challenge, in particular, in the case of a traveling-wave output structure that usually consists of a set of coupled cavities and an output arm, driven by an initially bunched beam [29]. Its advantage may be attributed to the distributed interaction along one or more radiation wavelengths, but at the same time, its drawback is its scaling with frequency that in an ordinary system is similar to that of klystrons.

Manuscript received September 25, 1999; revised March 22, 2000. This work was supported by the United States Department of Energy and the United States Air Force, under the High Power Microwave MURI program.

S. Banna and L. Schächter are with the Department of Electrical Engineering, Technion—Israel Institute of Technology, 32000 Haifa, Israel.

J. A. Nation and P. Wang are with the School of Electrical Engineering, Cornell University, Ithaca, NY 14853 USA.

Publisher Item Identifier S 0093-3813(00)05717-9.

Most of the experimental and theoretical efforts in the last decade were directed toward X-band operation [1]–[3], [5], [24], [25], [30]–[35]; however, the demand for high gradients at higher and higher frequencies for the next linear collider (NLC) pushes the operating frequency toward the Ka-band (e.g., 35 GHz), and as a result, this study focuses on this frequency regime [36]–[38]. The same trend is also motivated by a military need to deposit a large amount of energy in a relatively small area far away from the source—obviously, this ability is improved at higher frequencies.

Theoretical analysis [36] and preliminary experimental studies [37] indicated the feasibility of a 35-GHz traveling-wave amplifier based on a set of coupled cavities when only the symmetric mode was considered. We found that the difficulty with the scaling up the frequency is associated with beam power requirements. In order to benefit from the frequency increase, the rf power has to remain the same as in X-band; therefore, assuming similar efficiencies, the power carried by the beam has to be virtually identical. However, the scaling up in frequency dictates that the internal radius of the structure should scale down inversely proportional to the increase in frequency. This implies a similar change in the radius of the beam, which is difficult to envision because it entails an increase by a factor of 10 in the current density (assuming we preserve both the diode voltage and current). Although improving the cathode's material so that it withstands higher current density may result in a slightly higher current, the main alternative is a higher (electrostatic and magnetic) compression ratio. Yet, at several hundred amperes, it is difficult to envision an increase by an order of magnitude in the existing ratio. Even if this was possible, the problem of the magnetic field's necessity to guide the beam and the latter's expansion in the interaction process still remains [38]. In order to have some feeling regarding the implications of these constraints, consider an X-band structure (say, $35/3 = 11.66$ GHz) that may have a typical internal radius of 7 mm when driven by a beam of 3-mm radius. Requiring equal power levels carried by the beam for a system operating at Ka-band (35 GHz) and adopting the frequency scaling, which entails a beam of 1-mm radius, the necessary compression ratio should be increased by nine. As indicated, we belive that this may prove to be very difficult for a realistic device. A compression by a factor of two is feasible, thus implying a 2-mm radius for the beam. Moreover, to allow sufficient gap between the beam and the structure (for beam expansion), an internal radius of 3.5 mm for the structure seems to be a reasonable choice. This radius is almost by 50% larger than the simple frequency-scaling criterion implies.

Its implications on the operation of the symmetric transverse magnetic (TM) mode are high group velocity and low interaction impedance; these implications were discussed in [36], where the one-dimensional (1-D) macro particle approach was extended to two-dimensional (2-D), i.e., longitudinal and radial motion.

An additional implication of relatively large internal radius is proximity of other modes, in particular, of the asymmetric modes, to the TM_{01}-mode. Although in principle both the slow wave structure and its driving beam are azimuthally symmetric, asymmetry in the system may occur either because of the input or the output arm, uneven azimuthal electron distribution, or beam misalignment. A *longitudinally* modulated beam may couple energy from the main interacting symmetric mode to an asymmetric mode because of any of these mechanisms. Such modes are a linear combination of both TM and transverse electric (TE) modes, and for this reason, they are called hybrid electric and magnetic (HEM) modes; cold electromagnetic calculations indicate that the larger the internal radius of the structure, the bigger the frequency range where the lower symmetric and asymmetric modes overlap. From the perspective of the interaction with the electrons, the main problem with an asymmetric mode is that it has a nonzero TM field on axis, and as a result, electrons that move at relativistic velocities in the longitudinal direction may be deflected toward the structure. This effect is well known in the accelerator community [39]–[41] under the name of beam break-up (BBU), and substantial efforts are directed for its suppression in the NLC's acceleration structure [42].

Recently, pulse shortening was observed in high-power traveling-wave amplifier experiments conducted at Cornell University [43], and this triggered the current study in which we examine to what extent the HEM-mode contributes to the beam deflection to the wall in an *amplifier*. The build-up of asymmetric modes as a very narrow bunch traverses an *acceleration structure* was analyzed, but to the best of our knowledge, no equivalent analysis corresponds to a traveling-wave amplifier, where several major differences exist: each bunch in an amplifier is of the order of the wavelength, whereas in an accelerator, the bunch is at least ten times smaller. The transverse size of the beam in an amplifier is several millimeters larger than it is in an accelerator. In an amplifier, *collective* effects play a dominant role in the interaction and a guiding magnetic field exists—neither of the two exist in an accelerator. The interaction length is much shorter and the group velocity much higher in an amplifier compared with an accelerator; moreover, in the present analysis, the group velocity in the amplifier is assumed to be positive, whereas in an accelerator, this is in many cases negative. Finally, the number of bunches (pulse duration) in the interaction region is much larger in the case of an amplifier.

In this study, we investigate several aspects associated with the operation of a high-power traveling-wave amplifier operating at 35 GHz, also taking into consideration the lowest asymmetric mode. For this purpose, we have developed a quasi-analytic three-dimensional (3-D) model of the interaction of an ensemble of electrons with symmetric and asymmetric modes, specifically with TM_{01} and the low branch of HEM_{11}. Within the framework of this model, the full 3-D motion of the particles is calculated; however, their effect on the electromagnetic field is assumed to be only in the longitudinal direction (1-D). Additional assumptions of the model include positive group velocity of both modes, their basic functional form is preserved, the energy conversion is primarily controlled by the longitudinal motion, and no electrons are reflected. Our first step is to compare the impact of the asymmetric modes on the electrons' dynamics of two amplifiers, one driven by a *uniform* beam and the other by a (longitudinally) *bunched* beam. It is shown that the sensitivity of the former to the presence of the HEM_{11} is higher. Secondly, we investigate the impact of the HEM_{11} on the system's performance in both ways of excitation. Specifically, we check the sensitivity of the system to its main parameters, such as guiding magnetic field, beam's properties, and the power level of the HEM_{11} at the input. The extent the HEM_{11}-mode is destructive is quantified by the increase in the effective radius of the beam. In the last stage, we present a way for suppressing the HEM_{11}-mode.

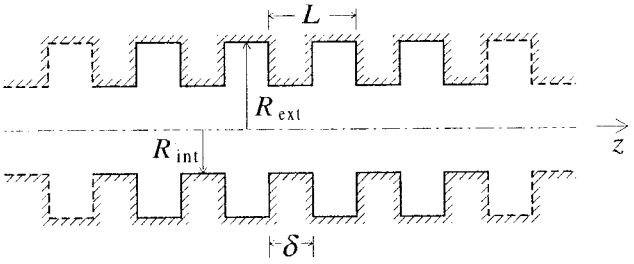

Fig. 1. Typical configuration of traveling-wave structure. $R_{\rm int}, R_{\rm ext}$ are the disk internal and external radii, respectively. L is the structure periodicity, and δ is the disk thickness.

II. Dynamics of the System

A uniform beam or an initially bunched beam, generated by either a series of cavities (klystron) or a slow-wave structure, is injected into a uniform disk-loaded periodic structure like the one illustrated in Fig. 1. The structure is designed so that the phase velocity of the interacting wave that is injected into the structure or generated by a bunched beam is synchronized to the average velocity of the electrons. The main interacting wave is the TM_{01}-mode, but as mentioned in the introduction, because of asymmetries of the structure or the beam, we assume that one asymmetric mode may develop. Moreover, when we refer in what follows to a prebunched beam, we assume axial bunching but uniform azimuthal distribution of particles. According to the dispersion curves [44], the closest asymmetric mode to the TM_{01} that may interact with the beam is the low branch of the HEM_{11}-mode. In the beam absence, all components of the electromagnetic field of both modes may be derived from the longitudinal components given by

$$\begin{aligned}
E_z^{(\mathrm{TM}_{01})}(r\phi,z;t) &= \mathcal{E}_1 \mathrm{I}_0(\Gamma_1 r)\cos(\omega_1 t - k_1 z - \psi_1)\\
H_z^{(\mathrm{TM}_{01})}(r\phi,z;t) &\equiv 0\\
E_z^{(\mathrm{HEM}_{11})}(r\phi,z;t) &= \mathcal{E}_2 \mathrm{I}_1(\Gamma_2 r)\cos(\omega_2 t - k_2 z - \phi - \psi_2)\\
H_z^{(\mathrm{HEM}_{11})}(r\phi,z;t) &= \mathcal{H}_2 \mathrm{I}_1(\Gamma_2 r)\cos(\omega_2 t - k_2 z - \phi - \psi_2).
\end{aligned} \tag{1}$$

In these expressions, k_ν are the wavenumbers of both modes that are assumed to correspond to a phase velocity smaller than c; index $\nu = 1$ represents the TM_{01}-mode, and index $\nu = 2$ represents the HEM_{11}-mode; $\Gamma_\nu \equiv \sqrt{k_\nu^2 - (\omega_\nu/c)^2}$; $r = \sqrt{x^2+y^2}$; $\phi = \arctan(y/x)$, and $I_n(\xi)$ is the modified Bessel function of the first type and order n. Within the framework of the 3-D model, we make two basic assumptions: first, it is assumed that the effect of the beam on the electromagnetic field is only in the longitudinal direction, and second its functional form is preserved. In addition to the rf field, a dc guiding magnetic field B_0 is assumed to be uniform in space.

Another component of the electromagnetic field that acts on the electrons is caused by the dc collective effect of the electrons in the beam. In the absence of the radiation field, we may assume that the electron beam is *uniformly* distributed in the *transverse* directions. Its density, denoted by n_0, generates an electrostatic field that in turn affects the motion of each electron; this field is given by

$$\vec{E}^{(\mathrm{dc})} = -\frac{en_0}{2\epsilon_0}\left[x\vec{1}_x + y\vec{1}_y\right]. \tag{2}$$

Furthermore, because the average velocity of the beam is v_0, the magnetic field associated with this motion in the beam domain is given by

$$\vec{H}^{(\mathrm{dc})} = \frac{en_0v_0}{2}\left[y\vec{1}_x - x\vec{1}_y\right]. \tag{3}$$

Consequently, the total electromagnetic field is composed of three components, the rf field, the dc collective field, and the magnetic guiding field

$$\begin{aligned} E_x &= E_x^{(\mathrm{rf})} + E_x^{(\mathrm{dc})}, \quad E_y = E_y^{(\mathrm{rf})} + E_y^{(\mathrm{dc})} \\ H_x &= H_x^{(\mathrm{rf})} + H_x^{(\mathrm{dc})} \\ E_z &= E_z^{(\mathrm{rf})}, \quad H_y = H_y^{(\mathrm{rf})} + H_y^{(\mathrm{dc})} \\ H_z &= H_z^{(\mathrm{rf})} + B_0/\mu_0. \end{aligned} \tag{4}$$

A. Transverse Motion

From these expressions, we can readily determine the equations of the transverse motion of the ith electron; they are given by

$$\begin{aligned} \frac{d}{dt}(\gamma_i\beta_{x,i}) &= \frac{1}{mc}\left[F_{x,i}^{(\mathrm{rf})} + F_{x,i}^{(\mathrm{dc})} - ec\beta_{y,i}B_0\right] \\ \frac{d}{dt}(\gamma_i\beta_{y,i}) &= \frac{1}{mc}\left[F_{y,i}^{(\mathrm{rf})} + F_{y,i}^{(\mathrm{dc})} + ec\beta_{x,i}B_0\right] \end{aligned} \tag{5}$$

where $F_{x,i}^{(\mathrm{rf})}, F_{y,i}^{(\mathrm{rf})}, F_{x,i}^{(\mathrm{dc})}$, and $F_{y,i}^{(\mathrm{dc})}$ are the transverse forces associated with the rf and dc electromagnetic fields, respectively. Based on (4), these forces are given by

$$\begin{aligned} F_{x,i}^{(\mathrm{rf})} &= -e\left[E_{x,i}^{(\mathrm{rf})} + c\mu_0\beta_{y,i}H_{z,i}^{(\mathrm{rf})} - c\mu_0\beta_{z,i}H_{y,i}^{(\mathrm{rf})}\right] \\ F_{x,i}^{(\mathrm{dc})} &= \frac{1}{2}m\omega_p^2\frac{1}{\gamma_{z,i}^2}x_i \\ F_{y,i}^{(\mathrm{rf})} &= -e\left[E_{y,i}^{(\mathrm{rf})} - c\mu_0\beta_{x,i}H_{z,i}^{(\mathrm{rf})} + c\mu_0\beta_{z,i}H_{x,i}^{(\mathrm{rf})}\right] \\ F_{y,i}^{(\mathrm{dc})} &= \frac{1}{2}m\omega_p^2\frac{1}{\gamma_{z,i}^2}y_i \end{aligned} \tag{6}$$

where $\gamma_{z,i} \equiv [1-\beta_{z,i}^2]^{-1/2}$ and $\omega_p \equiv \sqrt{e^2n_0/m\epsilon_0}$ is the plasma angular frequency.

In the expression for the rf forces, the second term may be neglected because the amplitude of all rf components are of the same order and for most practical purposes

$$|\beta_{x,i}|,\ |\beta_{y,i}| \ll |\beta_{z,i}|. \tag{7}$$

The transverse components of the rf electromagnetic field can be deduced from the Maxwell equation, and they are presented explicitly in the Appendix in terms of the amplitudes defined in (1). Equation (5) together with (6), (7), and (A.1)–(A.4) determine the transverse motion of the electrons in the presence of the electromagnetic field.

B. Poynting Theorem

After establishing the equations that determine the dynamics of the particles, we shall consider their effect on the dynamics of the rf field. Within the framework of the present model, we ignore the *direct* effect of the transverse motion on the energy exchange, and consequently, we shall consider only the longitudinal current density given by

$$\begin{aligned} &J_z(r,\phi,z;t) \\ &\quad = -e\sum_i v_{z,i}\frac{1}{r}\delta[r-r_i(t)]\delta[\phi-\phi_i(t)]\delta[z-z_i(t)] \end{aligned} \tag{8}$$

where $r_i(t), \phi_i(t)$, and $z_i(t)$ are the radial, azimuthal, and longitudinal location of the ith electron at any instant t; this assumption is consistent with the approximation described in (7). Thus, bearing in mind that the system operates in steady state and assuming that it remains in a linear regime (single frequency) at all times, the average power in each mode is determined by

$$\frac{d}{dz}\langle P(z)\rangle_t = -\int_{\mathrm{cs}} da\langle J_zE_z\rangle_t \tag{9}$$

where the integration is over the cross section (cs) of the wave guide and $\langle P(z)\rangle_t \equiv \langle\int_{cs} daS_z\rangle_t$ is the total power flow in each one of the modes. At this point, we introduce the concept of the interaction impedance that relates the average power flowing in the system, carried by the specific mode, with the amplitude of the longitudinal electric field (of the same mode), namely

$$\begin{aligned} Z_{\mathrm{int}}^{(\mathrm{TM}_{01})} &\equiv \frac{1}{2}\frac{\mathcal{E}_1^2(\pi R_{\mathrm{int}}^2)}{\langle P^{(\mathrm{TM}_{01})}(z)\rangle_t} \\ Z_{\mathrm{int}}^{(\mathrm{HEM}_{11})} &\equiv \frac{1}{2}\frac{\mathcal{E}_2^2(\pi R_{\mathrm{int}}^2)}{\langle P^{(\mathrm{HEM}_{11})}(z)\rangle_t} \end{aligned} \tag{10}$$

where R_{int} is the internal radius of the disk-loaded structure.

As already indicated, the interaction of both modes with the electrons is via longitudinal oscillations; in other words, this motion is the one that directly controls the interaction; however, indirectly, the transverse motion has a significant impact on the interaction because variation in the transverse location of the particles affects the interaction impedance and, thus, the coupling of the beam with the electromagnetic field. Based on these arguments and relying on (9), we conclude that the energy

stored in the symmetric mode is determined only by the symmetric current density, and therefore, the amplitude dynamics equation for the TM_{01}-mode is given by

$$\frac{d}{dz}\,\mathcal{E}_1^2(z) = \frac{2Z_{\rm int}^{(\rm TM_{01})}}{\pi R_{\rm int}^2}\,\frac{eN}{T}\,\mathcal{E}_1(z)\langle \mathrm{I}_0[\Gamma_1 r_i(z)] \cdot \cos[\omega_1\tau_i(z) - k_1 z - \psi_1(z)]\rangle_i \tag{11}$$

where we have integrated over time and beam's radius and denoted by N the number of particles in one period of the wave (T), $\tau_i(z)$ represents the time it takes the ith particle to reach the point z, and $r_i(z)$ is the radial location of the same particle at z.

We proceed by identifying the average current in one period of the wave as $I \equiv eN/T$ and adopting a complex notation, namely, $\overline{\mathcal{E}}_1 \equiv \mathcal{E}_1 e^{-j\psi_1}$. With this notation, the dynamics of the (complex) amplitude of the rf field as well as that of the phase, $\chi_{i,1}(z)$, of the ith particle relative to the TM_{01}-mode, is given by

$$\frac{d}{dz}\,\overline{\mathcal{E}}_1(z) = \frac{IZ_{\rm int}^{(\rm TM_{01})}}{\pi R_{\rm int}^2}\,\left\langle \mathrm{I}_0[\Gamma_1 r_i(z)] e^{-j\chi_{i,1}(z)}\right\rangle_i$$
$$\frac{d}{dz}\,\chi_{i,1}(z) = \frac{\omega_1}{c\beta_{z,i}} - k_1. \tag{12}$$

In a similar way, we may deduce the amplitude and the phase dynamics equation for the HEM_{11}-mode; the result is

$$\frac{d}{dz}\,\overline{\mathcal{E}}_2(z) = \frac{IZ_{\rm int}^{(\rm HEM_{11})}}{\pi R_{\rm int}^2}\,\left\langle \mathrm{I}_1[\Gamma_2 r_i(z)] e^{-j\chi_{i,2}(z)+j\phi_i(z)}\right\rangle_i$$
$$\frac{d}{dz}\,\chi_{i,2}(z) = \frac{\omega_2}{c\beta_{z,i}} - k_2 \tag{13}$$

where $\phi_i(z)$ is the azimuthal location of the ith particle. It is obvious from the amplitude equations that the coupling between the beam and the modes is controlled by the product $IZ_{\rm int}$, where (I) is a "beam" term and $(Z_{\rm int})$ is an "electromagnetic" term.

C. Energy Conservation

Following similar arguments as above, we may simplify the single particle energy conservation to read

$$mc^2\,\frac{d}{dt}\,\gamma_i(t) \simeq -e\,v_{z(t),i}E_z[r = r_i(t), \phi = \phi_i(t), z = z_i(t); t] \tag{14}$$

and using the complex notation previously introduced above, the single particle energy conservation may be written as follows:

$$\frac{d}{dz}\,\gamma_i(z) = -\frac{1}{2}\,\frac{e}{mc^2}\,\left\{\overline{\mathcal{E}}_1(z)\mathrm{I}_0\left[\Gamma_1 r_i(z)\right]e^{j\chi_{i,1}(z)} + \overline{\mathcal{E}}_2(z)\mathrm{I}_1\left[\Gamma_2 r_i(z)\right]e^{j\chi_{i,2}(z)-j\phi_i(z)} + \text{c.c.}\right\} \tag{15}$$

where rather than following the particles in time, we follow them in space, c.c. indicates the complex conjugate of the expression to the left bracket, and the relativistic factor γ_i is related to the transverse and longitudinal velocities by $\gamma_i = [1-\beta_{x,i}^2-\beta_{y,i}^2-\beta_{z,i}^2]^{-1/2}$.

In order to summarize the equations that describe the dynamics of the system, it is convenient to introduce a set of normalized quantities. We start by assuming that the interaction length is d, which allows us to determine the normalized coordinates $\xi \equiv z/d, \overline{x} \equiv x/d, \overline{y} \equiv y/d$, and as a result, the normalized radial location is $\overline{r} \equiv r/d$. The normalized field amplitude of the TM_{01} is denoted by $a_1 \equiv e\overline{\mathcal{E}}_1 d/mc^2$, whereas that of the HEM_{11} by $a_2 \equiv e\overline{\mathcal{E}}_2 d/mc^2$. Based on these definitions, the normalized coupling coefficients are

$$\alpha_1 \equiv \frac{eIZ_{\rm int}^{(\rm TM_{01})}}{mc^2}\,\frac{d^2}{\pi R_{\rm int}^2}$$
$$\alpha_2 \equiv \frac{eIZ_{\rm int}^{(\rm HEM_{11})}}{mc^2}\,\frac{d^2}{\pi R_{\rm int}^2} \tag{16}$$

and we define $\Omega_\mu = \omega_\mu d/c$, $K_\mu = k_\mu d$, $\mu = 1,2$, $\overline{\Gamma} \equiv \Gamma d, \Omega_c = ecB_0 d/mc^2$, and $\Omega_p^2 \equiv (eI\eta_0/mc^2)(d^2/\pi R_{\rm beam}^2)(1/\beta_{ph})$; $R_{\rm beam}$ is the radius of the beam at the input where it was injected. The normalized momentum $\overline{p}_{x,i} \equiv \gamma_i\beta_{x,i}$, $\overline{p}_{y,i} \equiv \gamma_i\beta_{y,i}$, and $\overline{p}_{z,i} \equiv \gamma_i\beta_{z,i}$ and the normalized rf forces are defined as follows:

$$\begin{aligned}
\overline{F}_{x,i}^{(\rm rf)} &\equiv \frac{F_x^{(\rm rf)}d}{mc^2} \\
&= A\left\{\left[\dot{\mathrm{I}}_0(\overline{\Gamma}_1\overline{r}_i)\,\mathrm{Re}\left(ja_1e^{j\chi_{i,1}}\right) + \dot{\mathrm{I}}_1(\overline{\Gamma}_2\overline{r}_i)\,\mathrm{Re}\left(ja_2e^{j\chi_{i,2}-j\phi_i}\right)\right]\cos(\phi_i) - \frac{\mathrm{I}_1(\overline{\Gamma}_2\overline{r}_i)}{\overline{\Gamma}_2\overline{r}_i}\,\mathrm{Re}\left(a_2e^{j\chi_{i,2}-j\phi_i}\right)\sin(\phi_i)\right\} \\
&\quad + B\left\{\left[\frac{\mathrm{I}_1(\overline{\Gamma}_2\overline{r}_i)}{\overline{\Gamma}_2\overline{r}_i}\,\mathrm{Re}\left(ja_2e^{j\chi_{i,2}-j\phi_i}\right)\right]\cos(\phi_i) - \dot{\mathrm{I}}_1(\overline{\Gamma}_2\overline{r}_i)\,\mathrm{Re}\left(a_2e^{j\chi_{i,2}-j\phi_i}\right)\sin(\phi_i)\right\} \\
\overline{F}_{y,i}^{(\rm rf)} &\equiv \frac{F_y^{(\rm rf)}d}{mc^2} \\
&= A\left\{\left[\dot{\mathrm{I}}_0(\overline{\Gamma}_1\overline{r}_i)\,\mathrm{Re}\left(ja_1e^{j\chi_{i,1}}\right) + \dot{\mathrm{I}}_1(\overline{\Gamma}_2\overline{r}_i)\,\mathrm{Re}\left(ja_2e^{j\chi_{i,2}-j\phi_i}\right)\right]\sin(\phi_i) + \frac{\mathrm{I}_1(\overline{\Gamma}_2\overline{\mathrm{r}}_\mathrm{i})}{\overline{\Gamma}_2\overline{\mathrm{r}}_\mathrm{i}}\,\mathrm{Re}\left(a_2e^{j\chi_{i,2}-j\phi_i}\right)\cos(\phi_i)\right\} \\
&\quad + B\left\{\left[\frac{\mathrm{I}_1(\overline{\Gamma}_2\overline{r}_i)}{\overline{\Gamma}_2\overline{r}_i}\,\mathrm{Re}\left(ja_2e^{j\chi_{i,2}-j\phi_i}\right)\right]\sin(\phi_i) + \dot{\mathrm{I}}_1(\overline{\Gamma}_2\overline{r}_i)\,\mathrm{Re}\left(a_2e^{j\chi_{i,2}-j\phi_i}\right)\cos(\phi_i)\right\}
\end{aligned} \tag{17}$$

where $A \equiv -\gamma_{ph}(1-\beta_{z,i}\beta_{ph})$, $B \equiv -j\mathcal{H}_0\gamma_{ph}(\beta_{ph}-\beta_{z,i})$, and $\mathcal{H}_0 \equiv \eta_0\mathcal{H}_2/\mathcal{E}_2$. With these definitions, we are now in position

to summarize the equations that describe the dynamics of the system; these read

$$\begin{aligned}
\frac{d}{d\xi}\left(\frac{a_1}{\sqrt{\alpha_1}}\right) &= \sqrt{\alpha_1}\left\langle \mathrm{I}_0(\overline{\Gamma}_1\overline{r}_i)\, e^{-j\chi_{i,1}}\right\rangle_i \\
\frac{d}{d\xi}\left(\frac{a_2}{\sqrt{\alpha_2}}\right) &= \sqrt{\alpha_2}\left\langle \mathrm{I}_1(\overline{\Gamma}_2\overline{r}_i)\, e^{-j\chi_{i,2}+j\phi_i}\right\rangle_i \\
\frac{d}{d\xi}\chi_{i,1} &= \frac{\Omega_1}{\beta_{z,i}} - K_1, \qquad \frac{d}{d\xi}\chi_{i,2} = \frac{\Omega_2}{\beta_{z,i}} - K_2 \\
\frac{d}{d\xi}\gamma_i &= -\frac{1}{2}\left[a_1\mathrm{I}_0(\overline{\Gamma}_1\overline{r}_i)\, e^{j\chi_{i,1}}\right. \\
&\quad \left. + a_2\mathrm{I}_1(\overline{\Gamma}_2\overline{r}_i)\, e^{j\chi_{i,2}-j\phi_i} + \text{c.c.}\right] \\
\frac{d}{d\xi}\overline{x}_i &= \frac{\beta_{x,i}}{\beta_{z,i}}; \qquad \frac{d}{d\xi}\overline{y}_i = \frac{\beta_{y,i}}{\beta_{z,i}} \\
\frac{d}{d\xi}\overline{p}_{x,i} &= -\Omega_c\frac{\overline{p}_{y,i}}{\overline{p}_{z,i}} + \Omega_p^2\frac{\overline{x}_i}{2\gamma_{z,i}^2\beta_{z,i}} + \frac{\overline{F}_x^{(\mathrm{rf})}}{\beta_{z,i}} \\
\frac{d}{d\xi}\overline{p}_{y,i} &= \Omega_c\frac{\overline{p}_{x,i}}{\overline{p}_{z,i}} + \Omega_p^2\frac{\overline{y}_i}{2\gamma_{z,i}^2\beta_{z,i}} + \frac{\overline{F}_y^{(\mathrm{rf})}}{\beta_{z,i}} \\
\overline{p}_{z,i} &= \sqrt{\gamma_i^2 - \overline{p}_{x,i}^2 - \overline{p}_{y,i}^2}.
\end{aligned} \tag{18}$$

Before we proceed to an analysis of the numerical solution of this set of equations for a practical system, it is important to point out that the approximations involved do not affect the global energy conservation. The latter is obtained by averaging the single particle energy conservation [fourth line in (18)] and substituting the equation for the expressions for the amplitude dynamics (first and second lines)

$$\frac{d}{d\xi}\left[\langle\gamma_i\rangle_i + \frac{1}{2\alpha_1}\,|a_1(\xi)|^2 + \frac{1}{2\alpha_2}\,|a_2(\xi)|^2\right] = 0. \tag{19}$$

III. Simulations Results and Discussion

Before introducing any of the simulations results, we would like to evaluate the *spatial growth* in the system. Based on (18), the spatial growth of the system may be deduced by taking twice the derivative of the amplitude equation and substituting in the equation of the motion; the result is

$$\begin{aligned}
&\frac{d^3a_1}{d\xi^3} + \frac{j}{2}\left[(\alpha_1\Omega_1p_1)a_1 + (\alpha_1\Omega_1U)a_2\right] \\
&\quad \cong -\alpha_1\left\langle\left(\frac{\Omega_1}{\beta_i} - K_1\right)^2 e^{-j\chi_{i,1}}\mathrm{I}_0(\overline{\Gamma}_1\overline{r}_i)\right\rangle \\
&\frac{d^3a_2}{d\xi^3} + \frac{j}{2}\left[(\alpha_2\Omega_2p_2)a_2 + (\alpha_2\Omega_2U^*)a_1\right] \\
&\quad \cong -\alpha_2\left\langle\left(\frac{\Omega_2}{\beta_i} - K_2\right)^2 e^{-j\chi_{i,2}+j\phi_i}\mathrm{I}_1(\overline{\Gamma}_2\overline{r}_i)\right\rangle
\end{aligned} \tag{20}$$

where

$$\begin{aligned}
U &\equiv \left\langle e^{-j(\chi_{i,1}-\chi_{i,2}+\phi_i)}\,(\gamma_i\beta_i)^{-3}\,\mathrm{I}_0\big(\overline{\Gamma}_1\overline{r}_i\big)\,\mathrm{I}_1\big(\overline{\Gamma}_2\overline{r}_i\big)\right\rangle \\
p_1 &\equiv \left\langle \mathrm{I}_0^2\big(\overline{\Gamma}_1\overline{r}_i\big)\,(\gamma_i\beta_i)^{-3}\right\rangle \\
p_2 &\equiv \left\langle \mathrm{I}_1^2\big(\overline{\Gamma}_2\overline{r}_i\big)\,(\gamma_i\beta_i)^{-3}\right\rangle
\end{aligned}$$

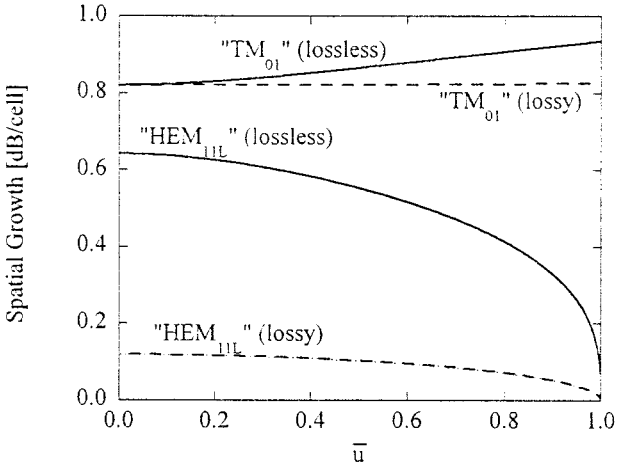

Fig. 2. The spatial growth per cell versus the coupling parameter $\overline{u}$ as defined in (4). Solid-line: growth rate without HEM-mode damping. Dashed-line: spatial growth with selective damping ($\overline{\sigma} \approx 0.05$).

and the terms where the phase varies rapidly were neglected. Ignoring the two "noise" terms in the right-hand side of both equations, we may calculate the eigenwavenumber of the coupled system by assuming solutions of the form $a_1 = \overline{a}_1 e^{-jS\xi}$ and $a_2 = \overline{a}_2 e^{-jS\xi}$; hence

$$\begin{pmatrix} S^3 + \frac{1}{2}\alpha_1\Omega_1p_1 & \frac{1}{2}\alpha_1\Omega_1U \\ \frac{1}{2}\alpha_2\Omega_2U^* & S^3 + \frac{1}{2}\alpha_2\Omega_2p_2 \end{pmatrix} \cdot \begin{pmatrix} \overline{a}_1 \\ \overline{a}_2 \end{pmatrix} = 0. \tag{21}$$

As clearly revealed by this matrix, the term U represents the coupling between the cold-structure eigenmodes (TM_{01} and HEM_{11}). From its definition, it is realized that U is determined by the correlation between the two phases $(\chi_{i,1}, \chi_{i,2})$ and by the correlation of the azimuthal, radial, and momentum distribution of the electrons. When the coupling between the modes is zero, each one of the modes (TM_{01} and HEM_{11}) develops independently according to $S^3 + S_1^3 = 0$ and $S^3 + S_2^3 = 0$, respectively, where $S_\mu^3 \equiv (1/2)\alpha_\mu\Omega_\mu p_\mu$. The coupling between the TM_{01} and HEM_{11} is controlled by a single parameter

$$\begin{aligned}
\overline{u} &\equiv \sqrt{\frac{UU^*}{p_1p_2}} \\
&= \frac{\left|\left\langle e^{-j(\chi_{i,1}-\chi_{i,2}+\phi_i)}\,(\gamma_i\beta_i)^{-3}\,\mathrm{I}_0\big(\overline{\Gamma}_1\overline{r}_i\big)\,\mathrm{I}_1\big(\overline{\Gamma}_2\overline{r}_i\big)\right\rangle\right|}{\sqrt{\left\langle \mathrm{I}_0^2\big(\overline{\Gamma}_1\overline{r}_i\big)\,(\gamma_i\beta_i)^{-3}\right\rangle\left\langle \mathrm{I}_1^2\big(\overline{\Gamma}_2\overline{r}_i\big)\,(\gamma_i\beta_i)^{-3}\right\rangle}}
\end{aligned} \tag{22}$$

because the solution of the coupled system can be determined from $S^3 + S_\pm^3 = 0$, where

$$S_\pm^3 = -\tfrac{1}{2}(S_1^3 + S_2^3) \pm \tfrac{1}{2}\sqrt{\left(S_1^3 - S_2^3\right)^2 + 4S_1^3S_2^3\,\overline{u}^2}. \tag{23}$$

In these expressions, S_+ corresponds to the HEM_{11}-like solution because at the limit $\overline{u} = 0$, $S_+ = S_2$, whereas S_- corresponds to the TM_{01}-like solution.

The solid lines in Fig. 2 illustrate the variation of the spatial growth per cell, $g_\pm \equiv (L/d)20\,\log(e^{\sqrt{3}S_\pm/2})$, as a function of the parameter $\overline{u}$. The parameters in this simulation are

$I = 300$ A, $V = 850$ kV, $R_{\rm int} = 3.5$ mm, $R_{\rm ext} = 5$ mm, $R_{\rm beam} = 2$ mm, $L = 1.98$ mm, $f_{\rm TM_{01}} = 35$ GHz, $f_{\rm HEM_{11}} = 38.63$ GHz, $Z_{\rm int}^{\rm TM_{01}} = 374\,\Omega$, $Z_{\rm int}^{\rm HEM_{11}} = 1.61$ kΩ, and it was assumed that the electrons have a vanishingly small velocity spread. When the modes are completely correlated ($\overline{u} = 1$), the spatial growth of the $\rm HEM_{11}$-like mode is zero, whereas the $\rm TM_{01}$-like is slightly larger than is the case when no coupling occurs ($\overline{u} = 0$). Although the $\rm HEM_{11}$-like wave becomes unimportant, we have to remember that the $\rm TM_{01}$-like mode is not a pure $\rm TM_{01}$-mode but rather a linear superposition of $\rm TM_{01}$ and $\rm HEM_{11}$; therefore, the impact of the HEM's components are destructive because they have the same spatial growth as the pure $\rm TM_{01}$ as they share the same eigenwavenumber.

In order to illustrate the impact of the coupled modes on the beam, we consider next the 3-D model to examine the development of the beam expansion. The first step is to compare the amplifier's performance with the asymmetric mode on and off. In all of the simulations that follow, we will discuss two different ways to drive the system. A $\rm TM_{01}$-wave at 35 GHz is injected into the structure, and it interacts with a *uniform* electron beam, or a *bunched* beam is injected into the structure, and no $\rm TM_{01}$ is explicitly launched; the beam modulation corresponds to the frequency of the $\rm TM_{01}$-mode. The beam expansion is described by the effective radius of the beam, defined as $\overline{r}_e \equiv R_e/R_{\rm int} = 2(d/R_{\rm int})\langle \overline{r}_i \rangle$; this definition complies with the result of uniform beam because $R_e = R_{\rm beam}$. Fig. 3 shows the effective radius of the beam's envelope for both ways of driving the system and for two different guiding magnetic fields $B_0 = 0.5, 1.5T$. Each frame consist of two curves describing the effective radius of the beam for both cases, when the HEM mode is turned on and off; the HEM power at the input end is 0.5 MW. The parameters used in this simulation are identical to those used in the calculation of the growth rate mentioned above and in addition $d = 2.6$ cm for bunched beam ($|\chi_{i,1}| < 7\pi/18$) and $d = 12$ cm for uniform beam. Throughout this study, the simulation is terminated if one particle reaches the internal radius of the structure; the location where this occurs is denoted by $z = z_t$. As revealed by these frames, three facts are evident. First, the relative impact of the HEM-mode on the transverse motion of the beam is more critical for uniform beam ($\sim$50% variation) than that for bunched beam in relative length terms; the absolute interaction length is longer in the case of the uniform beam. The length in both cases was chosen such that the interaction reaches saturation at the end of the structure. Second, when the HEM-mode is turned on, the simulation is terminated before the end of the structure; accordingly, the interaction process will be less efficient than when the HEM-mode is turned off. Third, even if the guiding magnetic field is very strong ($1.5T$), the impact of the HEM-mode is still considerable, especially for a uniform beam.

In order to have a better understanding of the system's dynamics, as revealed in part by Fig. 3, let us start and examine closely the sensitivity of the transverse motion of the beam to four main parameters of the system: HEM power level at the input, magnetic guiding field, beam's modulation, and beam's current. We are interested in three quantities that characterize the performance of the system: the effective radius of the beam ($\overline{r}_e$), the coupling parameter ($\overline{u}$), and the efficiencies of the modes defined as

$$\eta_{\rm TM_{01}}(\%) = \frac{100}{2\alpha_1}\frac{|a_1(\xi)|^2 - |a_1(\xi=0)|^2}{\langle \gamma_{i,in}\rangle_i - 1 + \dfrac{1}{2\alpha_1}|a_1(\xi=0)|^2 + \dfrac{1}{2\alpha_2}|a_2(\xi=0)|^2}$$
$$\eta_{\rm HEM_{11}}(\%) = \frac{100}{2\alpha_2}\frac{|a_2(\xi)|^2 - |a_2(\xi=0)|^2}{\langle \gamma_{i,in}\rangle_i - 1 + \dfrac{1}{2\alpha_1}|a_1(\xi=0)|^2 + \dfrac{1}{2\alpha_2}|a_2(\xi=0)|^2}. \quad (24)$$

Because the interaction does not always reaches the output end, it is convenient to define *normalized* efficiencies of both modes as the efficiency in the actual interaction length

$$\overline{\eta}_{\rm TM_{01}}(\%) = \frac{\eta_{\rm TM_{01}}(\%)}{z_{\rm t}/d}$$
$$\overline{\eta}_{\rm HEM_{11}}(\%) = \frac{\eta_{\rm HEM_{11}}(\%)}{z_{\rm t}/d}. \quad (25)$$

Next, we shall describe separately the impact of the asymmetric mode on beam's expansion for a uniform and for a bunched beam.

A. Uniform Beam

For testing the impact of the asymmetric mode on the dynamics of the electrons beam, we first investigate its build-up along the system. As already indicated, the latter may be initiated either by an asymmetry of the beam or of the structure, it may grow from noise, or it may develop from beam misalignment. Once initiated, the asymmetric mode starts to bounce between the two ends of the structure because in general [13], the latter is tuned to allow the symmetric mode to leave the system, but not necessarily the asymmetric mode. We introduce now the *overall reflection coefficient* (ρ) that represents the product of the reflections from both ends of the interaction region, the phase shift during one round trip and the attenuation associated with ohmic or other losses [13], [16], [17]. As this reflection coefficient is larger, the more rapid the build-up of the parasitic mode. Because a realistic beam pulse lasts for several hundreds of nanoseconds, time exists for several thousands of round-trips; thus, we shall consider in what follows a relatively large reflection coefficient ($\rho = 0.8, 0.9$) to reduce the number of round-trips the build-up occurs; the overall reflection coefficient of the symmetric mode is assumed to be zero.

Fig. 4 shows the build-up of the $\rm HEM_{11}$ power at the input versus the normalized location at the structure, wheras the number of round-trips is a parameter. The left frame shows the build-up of the power in the asymmetric mode for an overall reflection coefficient of $\rho = 0.8$; in the right frame, $\rho = 0.9$. In both frames, the $\rm TM_{01}$ power at the input is 5 kW and the guiding magnetic field is $B_0 = 1.5T$. This simulation result indicates that for a sufficiently high overall reflection coefficient, the asymmetric mode may reach very high power levels (100 MW) after a small number of round trips (4), (5). For a

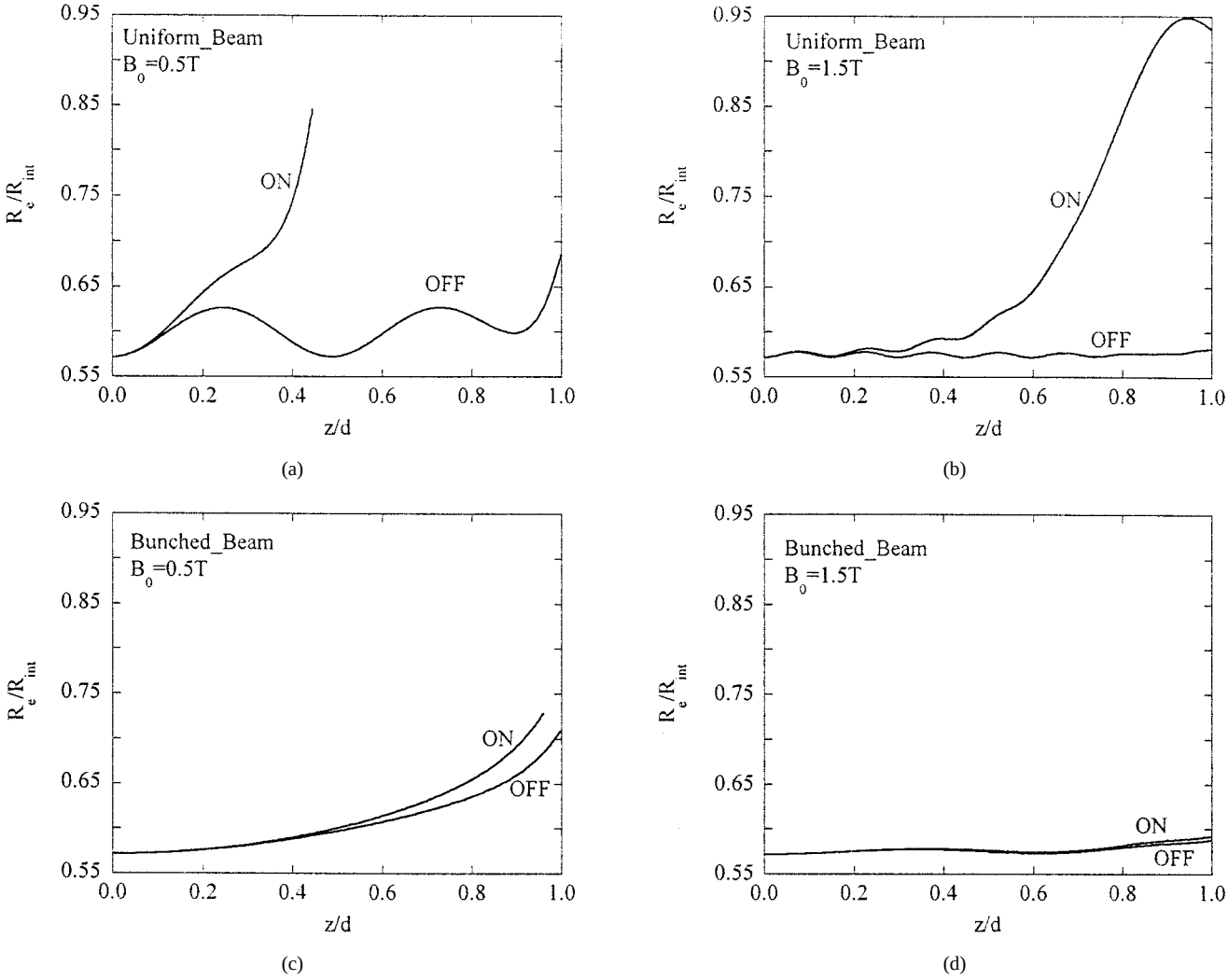

Fig. 3. The radius of the envelope for both cases: HEM_{11} is turned "off" and "on." (a) System driven by a uniform beam. (b) System driven by a bunched beam.

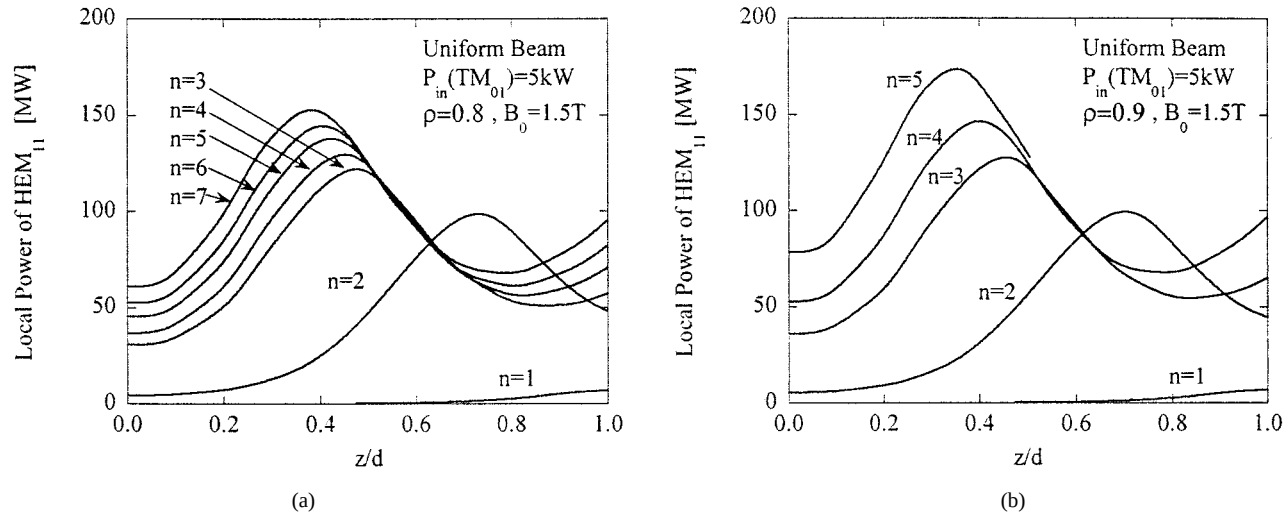

Fig. 4. The HEM_{11} output power for several number of round trips during the pulse duration. (a) Overall reflection coefficient (ρ) of 0.8. (b) Overall reflection coefficient (ρ) of 0.9.

smaller value of ρ, the build-up will occur on a longer time scale. The threshold for this phenomena is when the product of the one-pass gain of the asymmetric mode and the overall reflection coefficient equals unity; for values smaller than unity, no asymmetric mode will develop in the system [29].

Let us now examine more closely the interaction during a single-pass for a variety of HEM_{11} power levels at the input and different values of the guiding magnetic field. Fig. 5(a) shows the normalized efficiencies of both modes versus the guiding magnetic field. The input power of the TM_{01}-mode is 5-kW,

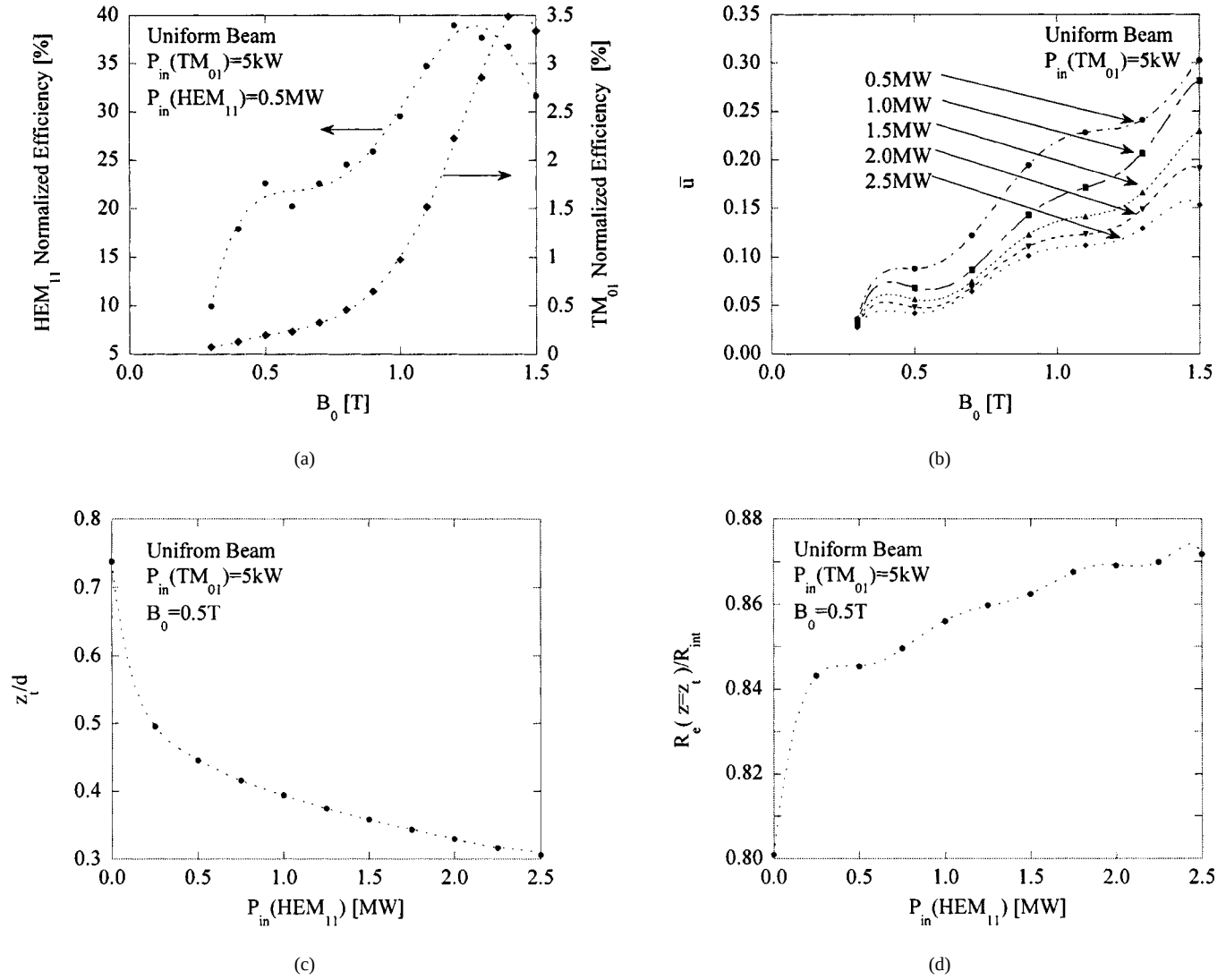

Fig. 5. Sensitivity of uniform beam to HEM_{11} input power level and guiding magnetic field. (a) The normalized efficiencies for both modes as a function of the guiding magnetic field; the simulation is terminated if electrons hit the wall. (b) The coupling parameter $\overline{u}$ versus the guiding magnetic field. (c) The normalized termination point z_t/d as a function of the initial HEM_{11} power level at the input. (d) The effective radius of the beam versus the HEM_{11} initial power level at the input.

and that of the asymmetric mode is 0.5-MW. This choice of the HEM power at the input is a byproduct of two constraints: first, we have just showed that for relatively high overall reflection coefficient (0.8–0.9), this power level is reasonable, and second, we intend to keep the numerical noise of the 10 000 particles to minimum and examine the impact of the HEM-mode on the interaction during *one* round-trip of the wave. Several results are evident, the normalized efficiency of the asymmetric mode is almost one order of magnitude higher than that of the symmetric mode; this is because intentionally the input power of the asymmetric mode was chosen to be two orders of magnitude larger than that of the symmetric mode to illustrate a possible scenario of a trapped mode. For high values of the guiding magnetic field, the normalized efficiency of both modes reaches high values because the simulation termination point is closer to the end of the structure because of the better confinement of the beam. Fig. 5(b) illustrates the coupling parameter versus the guiding magnetic field for several initial power levels of the asymmetric mode. As revealed by this graph, the coupling parameter varies monotonically as a function of the guiding magnetic field. For a specific magnetic field, the coupling parameter is higher when power of the HEM_{11}-mode at the input is smaller. Fig. 5(c) and (d) show the impact of the input power of the asymmetric mode on the interaction length. As we may anticipate, the length of the interaction is inversely proportional to the HEM_{11} power level at the input—see Fig. 5(c). Accordingly, Fig. 5(d) illustrates the expansion of the beam when the power level of the asymmetric mode at the input gets higher.

Next, we examine more closely the dynamics of the particles. Fig. 6 illustrates the phase-space distribution at the input and $z/d = 0.75$. Fig. 6(a) describes the phase-space at the input ($z/d = 0.0$), where the clusters are uniformly distributed in the domain $-\pi < \chi_1 < \pi$ and $|\gamma - 2.66| < 0.01$. The phase-space at the input is identical for both cases considered (HEM on or off). Fig. 6(b) shows the phase-space distribution after crossing 75% of the interaction region when the HEM_{11}

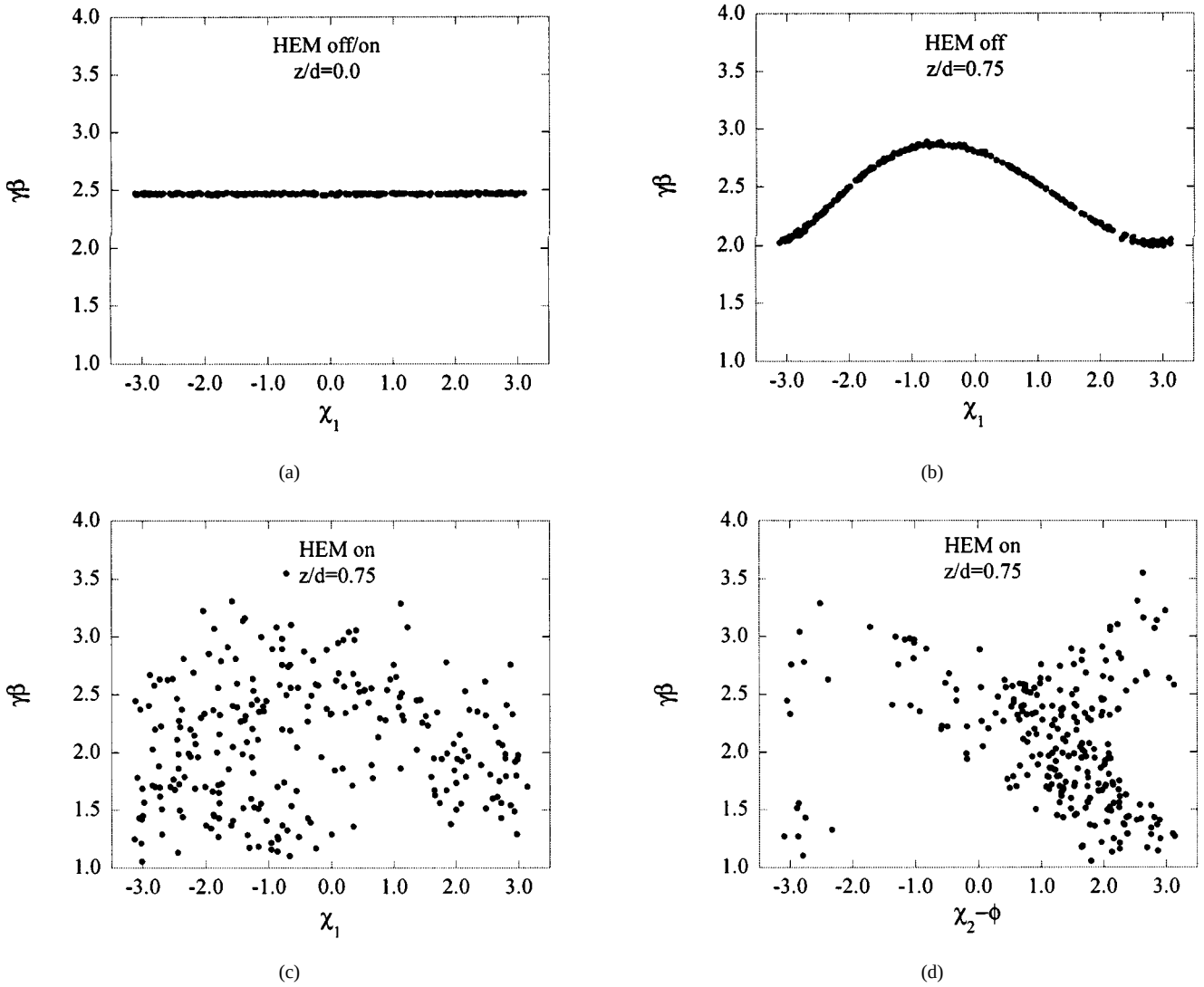

Fig. 6. Phase-Space distribution. (a) The phase-space distribution at $z/d = 0.0$. (b) The phase-space distribution at $z/d = 0.75$, HEM_{11} is turned "off." (c) The phase-space distribution at $z/d = 0.75$, when HEM_{11} is turned "on" and the phase of the particles is that relative to the TM_{01}-mode. (d) The phase-space distribution at $z/d = 0.75$, when HEM_{11} is turned "on" and the phase of the particles is that relative to the HEM_{11}-mode.

is turned off. The electrons in phase with the TM_{01} wave are decelerated, wheras those in antiphase are accelerated; nevertheless, the average energy is smaller, about 2.4, because part of it is transferred to the electromagnetic (EM) field. Note that the momentum spread at a given phase is virtually similar to that at the input, indicating that the beam is bunched at the frequency of the TM_{01}-mode. Fig. 6(c) and (d) show the phase-space distributions when the HEM_{11}-mode is turned on. Fig. 6(c) shows the phase-space versus χ_1, the phase of the particles relative to the TM_{01}-mode, for the same parameters as in the simulation in Fig. 6(b). Clearly, the symmetric mode is not the only one that determines the dynamics of the particles. In fact, Fig. 6(d), where the momentum of the ith particle is plotted as a function of its phase relative to the asymmetric mode, reveals a much organized phase-space. In spite of the change in the phase-space distribution, the average energy is similar to that calculated with the asymmetric mode off, but the spread at a given phase is significantly higher. In other words, the asymmetric mode, via the transverse motion, enhances the energy spread of particles that have the same phase relative to the symmetric mode. Moreover, the transverse motion (and, in particular, the radial component) causes particles to be close to the wall where the local rf forces are typically higher; consequently, the momentum (and energy) spread is larger.

B. Bunched Beam

Efficiencies of 25%–30% for a traveling-wave amplifier driven by a uniform beam are typical but not sufficient. Efficiency as high as 70% and even higher may in principle be achieved if the system is driven by a modulated beam, and high-order modes do not play a significant role [29]. In what follows, we shall investigate the impact of the asymmetric mode on the efficiencies of the symmetric mode, when the system is modulated at the frequency of the TM_{01}-mode. In the results of the simulations that follow, the input power of the TM_{01}-mode is zero, and the interaction length is $d = 2.6$ cm; all other parameters are as before.

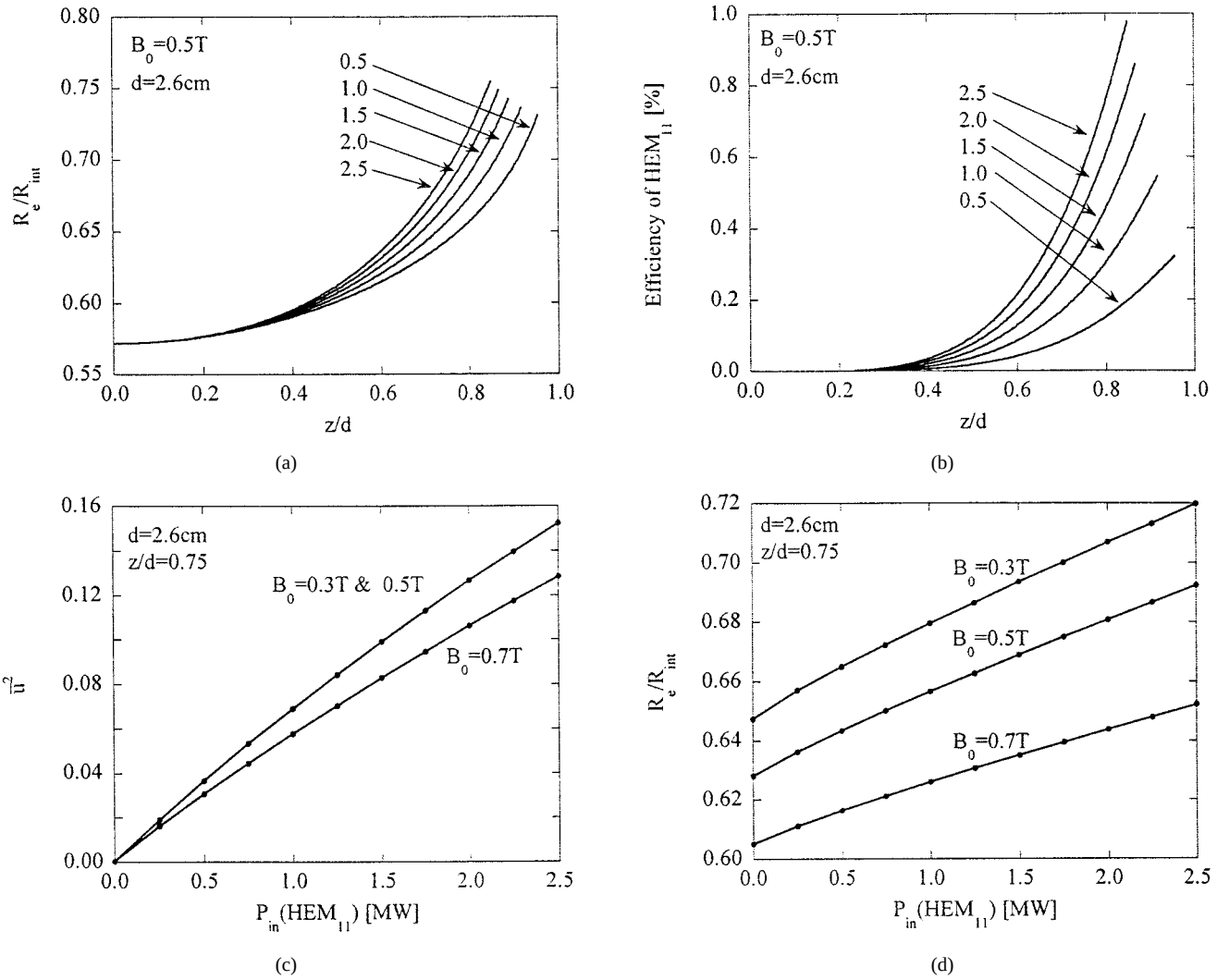

Fig. 7. Sensitivity to HEM_{11} power at the input (in MW). (a) The effective radius of the beam. (b) The efficiency of the HEM_{11} [%]. (c) The squared value of the coupling parameter ($\overline{u}$) for different values of the guiding magnetic field. (d) Beam radius for different values of the guiding magnetic field as a function of the power of the asymmetric mode at the input.

The first step is to check how the input power of the asymmetric mode affects the system's performance. Fig. 7(a) shows the effective radius of the beam for several initial HEM_{11} power levels at the input (0.5, 1.0, 1.5, 2.0, 2.5 MW); the TM_{01}-mode is generated by a modulated $|\chi_{i,1}| < 14\pi/18$ beam. We observe the monotonic increase of the beam radius along the interaction length up to the point where one particle hits the wall. The efficiency of the asymmetric mode is much lower than it is in the case of the uniform beam and it is higher as its initial power is larger—Fig. 7(b). Note that the higher the initial power of the asymmetric mode, the earlier the particles hit the wall. In Fig. 7(c) and (d), the effective radius of the beam and the coupling parameter are presented as function of the input power levels, where the guiding magnetic field is a parameter ($B_0 = 0.3, 0.5, 0.7T$). Fig. 7(c) shows the squared value of the coupling parameter ($\overline{u}$) at $z/d = 0.75$ versus the initial power of the HEM_{11}-mode. This quantity is almost linearly correlated to the HEM_{11} input power for a variety of guiding magnetic field values; the curve for $B_0 = 0.3T$ virtually overlaps the $B_0 = 0.5T$ data. In Fig. 7(d), we show the expansion of beam's radius versus the initial power of the asymmetric mode for different values of B_0 at the same point. The expansion of the beam is directly correlated with the variation of the coupling parameter and related linearly to the input power levels. A best fit of these simulations provides the following relations between the radius of the envelope and the input power of the asymmetric mode (in megawatts):

$$\begin{aligned}
\frac{R_e(\mathrm{B}_0 = 0.3T)}{R_{\mathrm{int}}} &= 0.0285 \times P_{in}(\mathrm{HEM}_{11}) + 0.649 \\
\frac{R_e(\mathrm{B}_0 = 0.5T)}{R_{\mathrm{int}}} &= 0.0254 \times P_{in}(\mathrm{HEM}_{11}) + 0.630 \\
\frac{R_e(\mathrm{B}_0 = 0.7T)}{R_{\mathrm{int}}} &= 0.0186 \times P_{in}(\mathrm{HEM}_{11}) + 0.606. \qquad (26)
\end{aligned}$$

According to these relations and assuming that the HEM power build-up is known, it is possible to estimate the location where electrons will hit the wall; again, we observe that by applying a stronger guiding magnetic field, we reduce the impact of the HEM_{11}-mode.

Our next step is to examine the effect of the modulation on the performance of the system. The left frame of Fig. 8 illus-

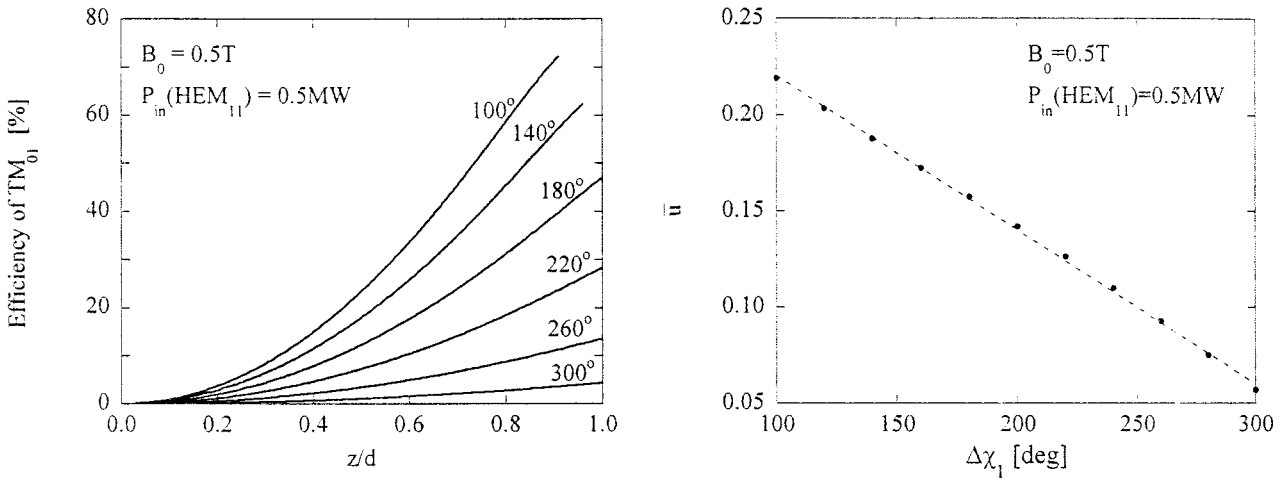

(a) (b)

Fig. 8. Sensitivity to the modulation of the beam. (a) Efficiency of TM_{01} [%] for different beam (initial) modulation. (b) The coupling parameter ($\overline{u}$) versus the beam's initial modulation.

trates the TM_{01} efficiency for a different beam's modulations ($\triangle\chi_1 = 100°, 140°, 180°, 220°, 260°, 300°$). In this simulation, the HEM_{11} power at the input is 0.5 MW and a guiding magnetic field of $0.5T$ is applied. It is a well-known fact that the efficiency associated with the symmetric mode is strongly dependent on the modulation of the beam at the corresponding frequency; this fact is also true in the presence of an asymmetric mode, as illustrated in Fig. 8(a), where high efficiencies ($\geq$70%) are achieved with a modulated beam ($\triangle\chi_{i,1} = 100°$). The main problem with high-modulated beams is the strong effect of the HEM_{11}-mode. For example, in the absence of the HEM_{11}-mode, the TM_{01} efficiency is about 80%, but with the former present [$P_{in}(\mathrm{HEM}_{11}) = 0.5$ MW], the simulation is terminated before reaching the end of the structure and the TM_{01} efficiency reaches only the 70% efficiency. The reduction in the symmetric mode efficiency may be more drastic because the HEM_{11} power may reach high levels, as we have already shown when investigating the build-up process. Moreover, the impact of the HEM_{11}-mode on the system's performance is directly correlated with the coupling parameter, and the latter is linearly correlated with phase-spread of the beam modulation, as illustrated in Fig. 8(b).

The relation between both parameters is given by

$$\overline{u} = 0.3 - 0.001 \triangle \chi_1 \tag{27}$$

where $\triangle\chi_1$ is expressed in degrees. From this last relation, it is obvious that any design has to be a tradeoff between two constraints; on the one hand, it is necessary to have small phase-spread to achieve high efficiency for the TM_{01}, and on the other hand, increase the phase-spread to reduce the coupling to the asymmetric mode and avoid beam interception at the wall. For this reason, in the last part of this section, we shall examine ways for suppressing the HEM_{11}-mode.

The last parameter we investigate is the current. Changing the beam's current affects both the interaction coupling coefficients (α_1 and α_2) given in (16), and as a result, the entire dynamics of the system varies. Fig. 9 shows the sensitivity of the coupling parameter and the effective radius to the current variations at $z/d = 0.5$. Both parameters are almost linearly proportional to the beam's current. Clearly, the impact of the HEM_{11} on the dynamics of the system is strongly related to the beam's properties (current and modulation), and again, in any design, we have to compromise between the same two constraints mentioned above.

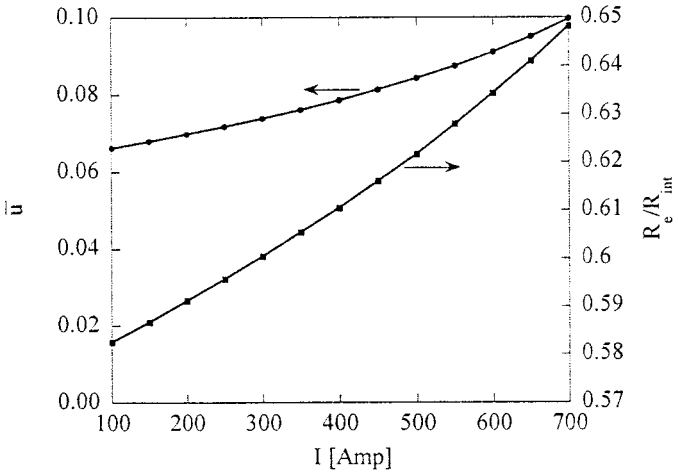

Fig. 9. The coupling parameter ($\overline{u}$) and the effective radius of the beam as a function of the current (in Amps); the TM_{01}-mode is generated by a modulated $|\chi_{i,1}| < 14\pi/18$ beam.

C. Asymmetric Mode Suppression

It is evident from the former results that the HEM_{11}-mode plays a destructive role during the interaction process. At best, it may prevent the system from reaching high efficiency, and at worst, it deflects the beam to the wall. In order to suppress the asymmetric mode, *selective* damping is required; by that, we mean that the damping mechanism is transparent to TM_{01}-mode [38], [42], [44]; however, it affects dramatically the asymmetric mode. In order to envision the impact of such a mechanism on the interaction process, we may represent this mechanism by a damping parameter, $\overline{\sigma}$, that in the absence of the beam causes

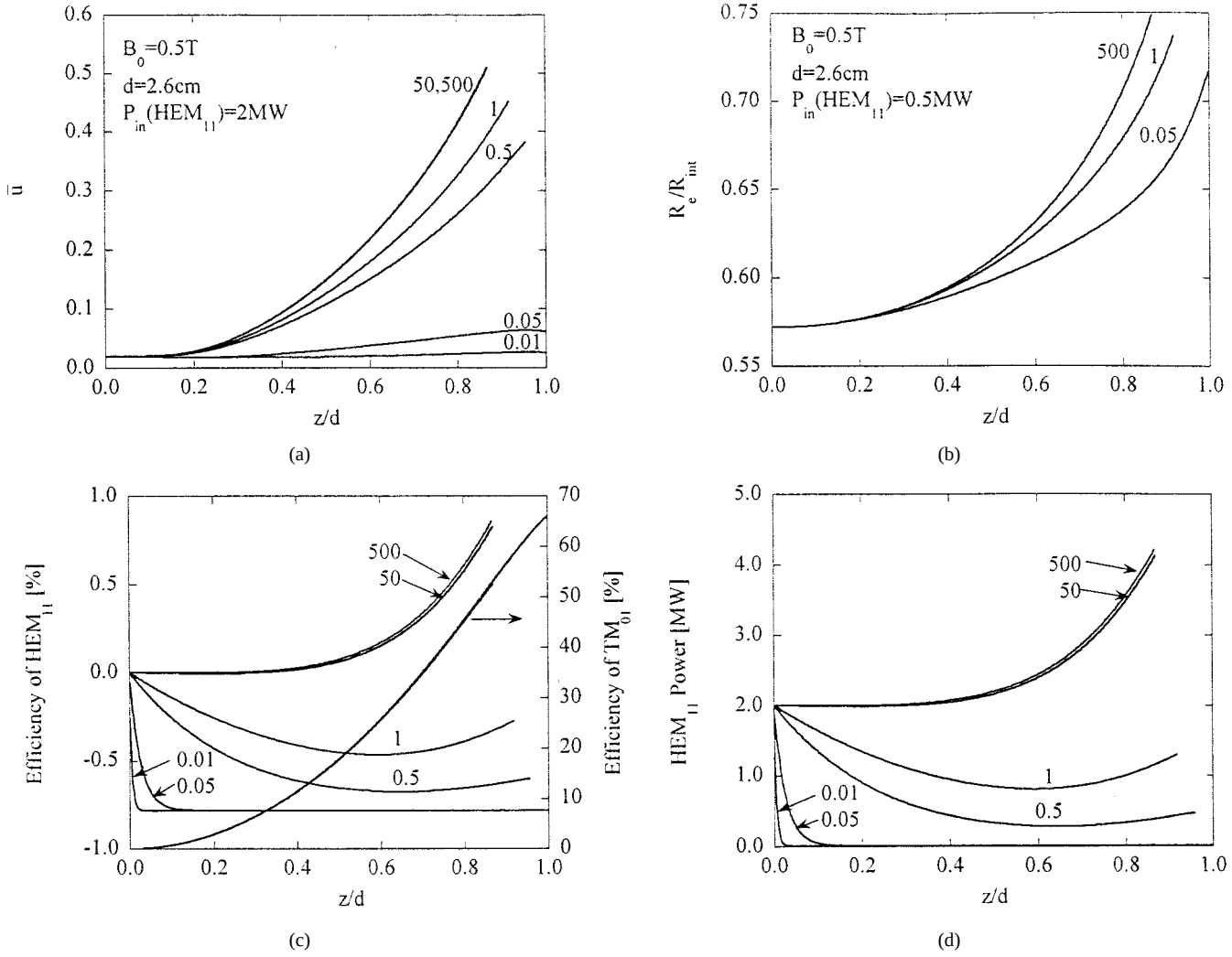

Fig. 10. (a) The coupling parameter for several values of the suppression parameter ($\overline{\sigma}$). (b) The effective radius of the beam. (c) The efficiencies of both modes (TM_{01} and HEM_{11}). (d) The HEM_{11} power (in MW); the TM_{01}-mode is generated by a modulated $|\chi_{i,1}| < 14\pi/18$ beam.

a decay corresponding to $e^{-\xi/\overline{\sigma}}$ of the asymmetric mode only. Consequently, in the amplitude equation of the HEM_{11}-mode, we may replace $(d\overline{a}_2/d\xi) \rightarrow (d\overline{a}_2/d\xi) + (1/\overline{\sigma})\,\overline{a}_2$; following the same approach as before, we find instead of (21)

$$\begin{pmatrix} S^3 + \frac{1}{2}\,\alpha_1\Omega_1 p_1 & \frac{1}{2}\,\alpha_1\Omega_1 U \\ \frac{1}{2}\,\alpha_2\Omega_2 U^* & S^3 + \frac{j}{\overline{\sigma}S^2} + \frac{1}{2}\,\alpha_2\Omega_2 p_2 \end{pmatrix} \cdot \begin{pmatrix} \overline{a}_1 \\ \overline{a}_2 \end{pmatrix} = 0. \tag{28}$$

This expression ignores the driving terms in (20) and is used to determine the eigenwavenumbers in a system with selective damping. The dashed lines in Fig. 2 illustrate the spatial growth per cell (in decibels) in the case of damping the HEM_{11}-mode ($\overline{\sigma} \approx 0.05$ corresponding to 1.7 dB per cell in the absence of the beam). Two facts are evident: first, the "HEM_{11}-like" mode is substantially suppressed, though not as we would expect from the cold attenuation; and second, the "TM_{01}-like" mode is almost independent of the $\overline{u}$, indicating that the "TM_{01}-like" is close to the pure TM_{01}-mode.

In Fig. 10, we compare the performance of the system for different values of the suppression parameter $\overline{\sigma}$ (0.01, 0.05, 0.5, 1, 50, 500). In Fig. 10(a), we show the coupling parameter variations for initial HEM_{11} power of 2 MW and guiding magnetic field of $0.5T$; this value is vanishingly small for $\overline{\sigma} = 0.01$, and it is well correlated with the envelope's radius variations shown in Fig. 10(b). Clearly, for values of $\overline{\sigma}$ of 0.05 or smaller, the beam in our system does not diverge. Both modes efficiencies are shown in Fig. 10(c). The HEM_{11} efficiency diminishes rapidly for small values of $\overline{\sigma}$, whereas the interaction of the TM_{01} is very efficient, reaching the 68% level when the HEM_{11} is well suppressed; for all of the values of $\overline{\sigma}$ plotted here, the curves of the TM_{01} efficiencies overlap; however, for high values of $\overline{\sigma}$, particles hit the wall; therefore, the system has to be shorter. Specifically, when $\overline{\sigma} = 500$, the TM_{01} efficiency reaches the 50% level before particles hit the wall, whereas for $\overline{\sigma} = 0.01$, it reaches the 68% level. The last graph shows the power associated with the HEM_{11}-mode. It is evident that the interaction of the HEM_{11}-mode with the electrons beam is not efficient at all for $\overline{\sigma} \leq 1$, and the damping along the structure is stronger than is the spatial growth associated with the interaction. This type of damping may be accomplished by a series choked-loaded [45]

cavities. These have a high quality factor (Q) at the frequency that corresponds to the TM_{01}-mode and low Q otherwise. Alternative ways of suppression of HEM-modes were discussed in [24], [25], and [42], and they include incoherence of the structure, namely, a structure that looks periodic to the symmetric mode but nonperiodic to the asymmetric one, differential extraction and absorption.

IV. Summary and Conclusion

A 3-D quasi-analytic model has been developed to investigate the impact of an asymmetric mode on the dynamics of an electrons beam injected into a traveling-wave amplifier. Based on this model, we were able to establish quantitative constraints to be imposed on the beam's properties and on the guiding magnetic field to obtain high TM_{01} efficiencies in spite of the presence of the HEM_{11}-mode. The asymmetric mode may grow from noise, and it may develop from slight asymmetry in the beam or its misalignment relative to the rf structure or the asymmetry associated with the input or output structure. The major drawback associated with its presence is its ability to enhance the beam blow-up in spite of the presence of a guiding magnetic field. Substantial reduction of the impact of the asymmetric mode is possible by selective and local damping. Specifically, here are the main conclusion of the present analysis:

- The coupling between symmetric and asymmetric mode is determined by one parameter $\overline{u}$, defined in (22); its value may vary from zero (no coupling) to unity in case of maximum coupling. If $\overline{u} = 1$, the components of the asymmetric mode grow in space at the same rate as these of the symmetric mode.
- The effective radius of the beam ($\overline{r}_e$) is dramatically affected by the asymmetric mode when the former is not modulated. For example, in the case of a uniform beam, electrons hit the structure after 40% of the interaction region (12 cm), whereas in the case of a prebunched beam, electrons almost hit the wall only after 90% of the interaction region (2.6 cm); the length in both cases was chosen such that the TM_{01}-mode reaches saturation in the absence of the asymmetric mode. Note that the absolute interaction length is longer in the case of a uniform beam.
- The build-up of the asymmetric mode is controlled by the overall reflection coefficient (from both ends), its spatial growth-rate, and the local attenuation.
- In case of an initially *uniform* beam and for a given input power (in both modes), the normalized efficiency (25) grows with the increasing guiding magnetic field. The efficiency of the asymmetric mode may be substantially higher than that of the symmetric mode because the former's power at the input may be significantly larger than the later's. The coupling parameter $\overline{u}$ is roughly linear with a guiding magnetic field. For a given guiding field, the beam radius increases linearly with the initial power of the asymmetric mode.
- In case of a *bunched* beam, the efficiency of the symmetric mode may be substantially larger than that of the asymmetric mode, the radius of the beam is proportional to the later's power, and the coupling parameter scales as the square root of this HEM_{11} power. This parameter is linear with the initial phase-spread of the bunch; it decreases as this phase-spread grows. Both the beam radius and the coupling parameter grow monotonically with the beam current.

Appendix

Using Ampere's and Faraday's laws and the expression for the longitudinal components of the EM field given in (1), we may deduce the transverse components of the EM field; the result is

$$\begin{aligned} E_{x,i}^{(\mathrm{rf})} =& -\gamma_{ph}\mathcal{E}_1\dot{\mathrm{I}}_0(\Gamma_1 r_i)\sin(\omega_1 t - k_1 z_i - \psi_1)\cos(\phi_i) \\ &+ \frac{1}{r_i}\frac{c}{\omega_2}\gamma_{ph}^2\beta_{ph}\mathrm{I}_1(\Gamma_2 r_i)\cos(\omega_2 t - k_2 z_i - \phi_i - \psi_2) \\ &\cdot[\beta_{ph}\eta_0\mathcal{H}_2\cos(\phi_i) - \mathcal{E}_2\sin(\phi_i)] \\ &-\gamma_{ph}\dot{\mathrm{I}}_1(\Gamma_2 r_i)\sin(\omega_2 t - k_2 z_i - \phi_i - \psi_2) \\ &\cdot[\beta_{ph}\eta_0\mathcal{H}_2\sin(\phi_i) + \mathcal{E}_2\cos(\phi_i)] \end{aligned} \tag{A.1}$$

$$\begin{aligned} E_{y,i}^{(\mathrm{rf})} =& -\gamma_{ph}\mathcal{E}_1\dot{\mathrm{I}}_0(\Gamma_1 r_i)\sin(\omega_1 t - k_1 z_i - \psi_1)\sin(\phi_i) \\ &+ \frac{1}{r_i}\frac{c}{\omega_2}\gamma_{ph}^2\beta_{ph}\mathrm{I}_1(\Gamma_2 r_i)\cos(\omega_2 t - k_2 z_i - \phi_i - \psi_2) \\ &\cdot[\beta_{ph}\eta_0\mathcal{H}_2\sin(\phi_i) + \mathcal{E}_2\cos(\phi_i)] \\ &+\gamma_{ph}\dot{\mathrm{I}}_1(\Gamma_2 r_i)\sin(\omega_2 t - k_2 z_i - \phi_i - \psi_2) \\ &\cdot[\beta_{ph}\eta_0\mathcal{H}_2\cos(\phi_i) - \mathcal{E}_2\sin(\phi_i)] \end{aligned} \tag{A.2}$$

$$\begin{aligned} H_{x,i}^{(\mathrm{rf})} =& \frac{1}{\eta_0}\gamma_{ph}\beta_{ph}\mathcal{E}_1\dot{\mathrm{I}}_0(\Gamma_1 r_i)\sin(\omega_1 t - k_1 z_i - \psi_1)\sin(\phi_i) \\ &- \frac{1}{r_i}\frac{c}{\omega_2}\gamma_{ph}^2\beta_{ph}\mathrm{I}_1(\Gamma_2 r_i)\cos(\omega_2 t - k_2 z_i - \phi_i - \psi_2) \\ &\cdot\left[\beta_{ph}\frac{\mathcal{E}_2}{\eta_0}\cos(\phi_i) + \mathcal{H}_2\sin(\phi_i)\right] \\ &-\gamma_{ph}\dot{\mathrm{I}}_1(\Gamma_2 r_i)\sin(\omega_2 t - k_2 z_i - \phi_i - \psi_2) \\ &\cdot\left[\beta_{ph}\frac{\mathcal{E}_2}{\eta_0}\sin(\phi_i) - \mathcal{H}_2\cos(\phi_i)\right] \end{aligned} \tag{A.3}$$

$$\begin{aligned} H_{y,i}^{(\mathrm{rf})} =& -\frac{1}{\eta_0}\gamma_{ph}\beta_{ph}\mathcal{E}_1\dot{\mathrm{I}}_0(\Gamma_1 r_i)\sin(\omega_1 t - k_1 z_i - \psi_1)\cos(\phi_i) \\ &- \frac{1}{r_i}\frac{c}{\omega_2}\gamma_{ph}^2\beta_{ph}\mathrm{I}_1(\Gamma_2 r_i)\cos(\omega_2 t - k_2 z_i - \phi - \psi_2) \\ &\cdot\left[\beta_{ph}\frac{\mathcal{E}_2}{\eta_0}\sin(\phi_i) - \mathcal{H}_2\cos(\phi_i)\right] \\ &-\gamma_{ph}\dot{\mathrm{I}}_1(\Gamma_2 r_i)\sin(\omega_2 t - k_2 z_i - \phi_i - \psi_2) \\ &\cdot\left[\beta_{ph}\frac{\mathcal{E}_2}{\eta_0}\cos(\phi_i) + \mathcal{H}_2\sin(\phi_i)\right] \end{aligned} \tag{A.4}$$

where $\beta_{ph} \equiv (\omega_1/ck_1) = (\omega_2/ck_2)$ is the normalized phase velocity, $\gamma_{ph} = 1/\sqrt{1-\beta_{ph}^2}$, and $\eta_0 \equiv \sqrt{\mu_0/\epsilon_0}$.

References

[1] G. Caryotakis, "High power microwave tubes: In the laboratory and on-line," *IEEE Trans. Plasma Sci.*, vol. 22, pp. 683–691, 1994.

[2] D. Sprehn, G. Caryotakis, E. Jongewaard, and R. Phillips, "Periodic permanent magnet development for liner collider X-band klystron," in *Proc. High Energy Density Microw., AIP Conf. 474*, 1998, p. 31.

[3] G. Caryotakis, G. Scheitrum, E. Jongewaard, A. Vlieks, W. R. Fowkes, L. Song, and J. Li, "High power W-band klystrons," in *Proc. High Energy Density Microw., AIP Conf. 474*, 1998, p. 59.

[4] R. Rossat *et al.*, "Demonstration of two-beam acceleration and 30 GHz power production in the CLIC test facility," in *Proc. High Energy Density Microw., AIP Conf. 474*, 1998, p. 23.

[5] Y. H. Chin *et al.*, "Development of the X-band RF power source for the JLC," in *Proc. 1999 Particle Accelerator Conf.*, New York, Mar. 29–Apr. 12 1999, p. 3414.
[6] G. A. Westenskow *et al.*, Progress on the relativistic klystron two-beam accelerator prototype, in Proc. Adv. Accelerator Concepts, 8th Workshop, AIP 472, Baltimore, MD, p. 983, 1998.
[7] M. Blank *et al.*, "Experimental demonstration of high-power millimeter wave gyro-amplifier," in *Proc. High Energy Density Microw., AIP Conf. 474*, 1998, p. 165.
[8] S. H. Gold *et al.*, "Status report on the 11.424GHz magnicon amplifier," in *Proc. High Energy Density Microw., AIP Conf. 474*, 1998, p. 179.
[9] O. A. Nezhevenko *et al.*, "X-band magnicon amplifier," in *Proc. 1999 Particle Accelerator Conf.*, New York, Mar. 29–Apr. 12 1999, p. 1049.
[10] E. B. Abubakirov *et al.*, "X-band amplification of gigawatt pulse power," in *Proc. High Energy Density Microw., AIP Conf. 474*, 1998, p. 360.
[11] M. Petelin *et al.*, "Quasi-optical components for MMW fed radars and particle accelerators," in *Proc. High Energy Density Microw., AIP Conf. 474*, 1998, p. 304.
[12] M. J. Arman, "High efficiency long pulse gigawatt sources of HPM radiation," in *Proc. High Energy Density Microw., AIP Conf. 474*, 1998, p. 342.
[13] W. Lawson *et al.*, High-power operation of the University of Maryland coaxial gyroklystron experiment, in Proc. Advanced Accelerator Concepts, 8th Workshop, AIP 472, Baltimore, MD, p. 128, 1998.
[14] D. Shiffler, J. D. Ivers, G. S. Kerslick, J. A. Nation, and L. Schächter, "A two stage high-power traveling-wave tube amplifier," *Appl. Phys Lett.*, vol. 58, pp. 899–901, 1991.
[15] ——, "A high power two stage traveling-wave tube amplifier," *J. Appl. Phys.*, vol. 70, pp. 106–113, 1991.
[16] T. J. Davis, J. A. Nation, and L. Schächter, "High power microwaves at 9GHz from an extended length cavity in a coaxial beam geometry," *Appl. Phys. Lett.*, vol. 63, pp. 1854–1856, 1993.
[17] ——, "Results from an X-band coaxial extended length cavity," *IEEE Trans. Plasma Sci.*, vol. 22, pp. 504–510, 1994.
[18] E. Kuang, T. J. Davis, G. S. Kerslick, J. A. Nation, and L. Schächter, "Transit time isolation of a high power microwave amplifier TWT," *Phys. Rev. Lett.*, vol. 71, pp. 2666–2669, 1993.
[19] ——, "Low group velocity traveling wave tube amplifier," *IEEE Trans. Plasma Sci.*, vol. 2, pp. 511–517, 1994.
[20] S. A. Naqvi, G. S. Kerslick, J. A. Nation, and L. Schächter, "Resonance shift in relativistic traveling wave amplifiers," *Phys. Rev. E*, vol. 53, pp. 4229–4231, 1996.
[21] ——, "Axial extraction of high-power microwaves from relativistic traveling wave amplifiers," *Appl. Phys. Lett.*, vol. 69, pp. 1550–1552, 1996.
[22] S. A. Naqvi, J. A. Nation, L. Schächter, and Q. Wang, "High efficiency TWT design using traveling-wave bunch compression," *IEEE Trans. Plasma Sci.*, vol. 26, pp. 840–845, 1998.
[23] G. Faillon, C. Bearzatto, and A. Beunas, "Long pulse and large bandwidth multi-beam klystron," in *Proc. High Energy Density Microw., AIP Conf. 474*, 1998, p. 107.
[24] J. Haimson and B. Meklenburg, "A CW nonsynchronous traveling wave structure for a 300MeV pulse strecher ring," in *Proc. 1987 IEEE Particle Accelerator Conf.*, 1987, p. 1919.
[25] ——, "Suppression of beam induced pulse shortening modes in high-power RF generators TW output structure," in *Proc. SPIE Symp. Intense Microw. Particle Beams II*, vol. 1629, Los Angeles, CA, 1992, p. 209.
[26] J. Haimson, B. Meklenburg, and B. Danley, "Initial performance of a high-gain, high-efficiency 17GHz traveling wave relativistic klystron for high gradient acceleration research," in *Proc. Pulse RF Sources for Linear Colliders, AIP Conf. 337*. New York: AIP Press, 1995, p. 146.
[27] O. A. Nezhevenko, V. P. Yaovlev, A. K. Ganguly, and J. L. Hirshfield, "High-power pulsed magnicon at 34GHz," in *Proc. High Energy Density Microw., AIP Conf. 474*. New York: AIP Press, 1998, p. 195.
[28] F. Mako, L. K. Len, and W. Peter, "Self-bunching electron guns," in *Proc. Adv. Accelerator Concepts, 8th Workshop*, Baltimore, MD, 1998, p. 983.
[29] L. Schächter, "High efficiency beam-wave interaction in quasiperiodic structures," *Phys. Rev. E.*, vol. 52, pp. 2037–2044, 1995.
[30] L. Schächter, J. A. Nation, and G. S. Kerslick, "On the bandwidth of short traveling wave tubes," *J. Appl. Phys.*, vol. 68, pp. 5874–5882, 1990.
[31] L. Schächter, "Cerenkov traveling wave tube with a spatially varying dielectric coefficient," *Phys. Rev. A*, vol. 43, pp. 3785–3794, 1991.
[32] L. Schächter, J. A. Nation, and D. Shiffler, "Theoretical studies of high-power Cerenkov amplifiers," *J. Appl. Phys.*, vol. 70, pp. 114–124, 1991.
[33] L. Schächter and J. A. Nation, "An analytical method for studying quasiperiodic disk loaded waveguide," *Appl. Phys. Lett.*, vol. 63, pp. 2441–2443, 1993.
[34] ——, "Propagation of electromagnetic and space charge waves in quasi-periodic structures," *Phys. Plasmas*, vol. 2, pp. 889–901, 1995.
[35] ——, "Slow wave amplifiers and oscillators: A unified study," *Phys. Rev. A.*, vol. 45, pp. 8820–8832, 1992.
[36] ——, "Beam-quality and guiding magnetic field requirements for a high-power traveling wave amplifier operating at 35GHz," *Phys. Rev. E*, vol. 57, pp. 7176–7183, 1998.
[37] Cz. Golkowski, J. D. Ivers, J. A. Nation, P. Wang, and L. Schächter, "First results from a high-power KA-band TWT," in *Proc. PAC'99 Particle Accelerator Conf.*, New York, 1999, p. 3603.
[38] S. Banna, J. A. Nation, L. Schächter, and P. Wang, The coupling of TM_{01} and HEM_{11} in a high-power, high-efficiency traveling wave amplifier, submitted for publication.
[39] W. K. H. Panofsky and W. A. Wenzel, Some consideration concerning the transverse deflection of charged particles in radio frequency fields, in Rev. Sci. Instr., vol. 27, p. 967, 1956.
[40] R. H. Helm and G. Loew, "Beam break-up," in *Linear Accelerators*, P. M. Lapostolle and A. L. Septier, Eds. Amsterdam: North Holland, 1970, p. 173.
[41] Y. Y. Lau, "Classification of beam break-up instabilities in linear accelerators," *Phys. Rev. Lett.*, vol. 53, pp. 1141–1144, 1989.
[42] R. M. Jones, N. M. Kroll, and R. H. Miller, "Including internal losses in the equivalent circuit model of the SLAC damped detuned structure (DDS)," in *Proc. PAC'99, Particle Accelerator Conf.*, New York, 1999, p. 3471.
[43] P. Wang, J. D. Ivers, J. A. Nation, S. Banna, and L. Schächter, "A comparative study of high power, multistage TWT amplifiers," in *Proc. PAC'99, Particle Accelerator Conf.*, New York, 1999, p. 3600.
[44] S. Banna, J. A. Nation, L. Schächter, and P. Wang, "Interaction of TM_{01} and HEM_{11} in a TWT," in *Proc. PAC'99, Particle Accelerator Conf.*, New York, 1999, p. 3609.
[45] T. Shintake, "The Choke Mode Cavity," *Jpn. J. Appl. Phys.*, pp. 1567–1531, 1992.

Samer Banna (S'93–M'96) was born in Nazareth, Israel, in 1975. He received the B.Sc. and M.Sc. degrees from the Technion-Israel Institute of Technology in electrical engineering, in 1997 and 2000, respectively. He is currently pursuing the Ph.D. degree in electrical engineering at the Technion.

John A. Nation (SM'76–F'89) completed his Ph.D degree in 1960 from Imperial College. He joined the Plasma Physics group in Frascati, Italy, where he worked on a theta pinch device. In 1962, he returned to the U.K. as a Staff Member at the Central Electricity Generating Board research laboratories. Since 1965, he has been at Cornell University where he is a Professor of Electrical Engineering. He was Director of the School of Electrical Engineering from 1984 to 1989. He is a Fellow of both the IEEE and the American Physical Society. He was one of the founder members of the Laboratory of Plasma Studies at Cornell and has been actively involved, through the laboratory, in the direction of its intense particle beam research program. His principal research interests are in pulse power technology and its applications to particle accelerators.

Levi Schächter (M'97–SM'99) graduated from the EE (B.Sc, M.Sc., and D.Sc.) and Physics (B.A.) Departments of the Technion (1983, 1985, and 1988). After his graduated studies, he was engaged in research during four years at Cornell University on high power microwave radiation sources for future accelerators as well as electron sources for radiation sources. Currently he is an Associate Professor with the EE Department of the Technion. His main fields of interest are: Radiation sources based on free electrons and advanced aceleration concepts. At the Technion, he established theoretical and experimental activity on radiation and electron sources. During the years, he was awarded a number of prizes and fellowships for his research, among them: Guttwirth Prize, Fellowship of Japan Society for the Promotion of Science (JSPS), Rothschild Fellowship and IEEE Prize (Israel Branch). He holds the Louis and Miriam Benjamin Academic Lectureship and he is a Member of the American Physical Society, IEEE and URSI.

Pingshan Wang (M'71) was born in China, in 1965. He received the Ph.D. degree in physics from Tsinghua University, Beijing, China, in 1999. From 1993 to 1997, he was an Associate Professor at Institute of Applied Electronics, Sichuan, China. He also served as a Deputy General Engineer of the institute and the Director of the High Power Microwave Laboratory at the institute. He is currently a Visiting Scientist at Laboratory of Plasma Science, Cornell University, working on relativistic TWT amplifiers.